Smart Materials and Structures

Experimental study of a self-powered and sensing MR-damper-based vibration control system

Smart Mater. Struct. **20** (2011) 105007 (13pp) doi:10.1088/0964-1726/20/10/105007

Experimental study of a self-powered and sensing MR-damper-based vibration control system

Bogdan Sapiński

Department of Process Control, AGH University of Science and Technology, aleja Mickiewicza 30, 30-059 Cracow, Poland

E-mail: deep@agh.edu.pl

Received 11 March 2011, in final form 6 July 2011
Published 31 August 2011
Online at stacks.iop.org/SMS/20/105007

Abstract

The paper deals with a semi-active vibration control system based on a magnetorheological (MR) damper. The study outlines the model and the structure of the system, and describes its experimental investigation. The conceptual design of this system involves harvesting energy from structural vibrations using an energy extractor based on an electromagnetic transduction mechanism (Faraday's law). The system consists of an electromagnetic induction device (EMI) prototype and an MR damper of RD-1005 series manufactured by Lord Corporation. The energy extracted is applied to control the damping characteristics of the MR damper.

The model of the system was used to prove that the proposed vibration control system is feasible. The system was realized in the semi-active control strategy with energy recovery and examined through experiments in the cases where the control coil of the MR damper was voltage-supplied directly from the EMI or voltage-supplied via the rectifier, or supplied with a current control system with two feedback loops. The external loop used the sky-hook algorithm whilst the internal loop used the algorithm switching the photorelay, at the output from the rectifier. Experimental results of the proposed vibration control system were compared with those obtained for the passive system (MR damper is off-state) and for the system with an external power source (conventional system) when the control coil of the MR damper was supplied by a DC power supply and analogue voltage amplifier or a DC power supply and a photorelay.

It was demonstrated that the system is able to power-supply the MR damper and can adjust itself to structural vibrations. It was also found that, since the signal of induced voltage from the EMI agrees well with that of the relative velocity signal across the damper, the device can act as a 'velocity-sign' sensor.

(Some figures in this article are in colour only in the electronic version)

1. Introduction

There are two main goals in the field of harvesting energy from structural vibrations. The first is to extract energy from vibrations that can be used to power wireless sensors whilst the second is to provide the power source for vibration control systems. This study deals with the latter problem and is focused on semi-active magnetorheological (MR)-damper-based vibration control systems. Recently such systems have received significant attention because MR dampers offer the capability of active devices and have good performance, and low power requirements. The majority of these systems are feedback systems with external power supply units.

The last decade has witnessed a major interest in MR-damper-based vibration control systems with energy harvesting in which the external power supply part is replaced by the electromagnetic induction device (EMI) (figure 1). The EMI, composed of permanent magnets and a coil, converts mechanical into electrical energy, and produces current proportional to the rate of change of the movement of an

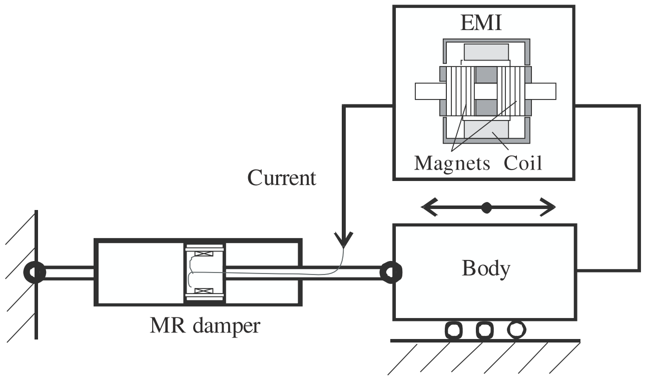

Figure 1. The MR-damper-based vibration control system with energy harvesting.

MR damper according to Faraday's law of electromagnetic induction. This energy is applied to control the damping characteristics of the MR damper attached to the EMI by the input current produced by the device.

The EMI can be used in the MR-damper-based vibration control system as a power source as well as a controller determining the command voltage input according to structural responses and that is why the system is referred to as a self-powered system. It is apparent that such a system is able to adjust itself to the structural vibrations and can be much more compact, convenient, and economic than conventional semi-active systems which need sensor(s), a controller, a current driver to activate the MR damper, and an external power supply unit.

The concept of active control with the harvested energy from structural vibrations and its use for powering the MR damper in civil engineering was first proposed by Scruggs and Lindner (1999). From that time a growing number of papers have been written on self-powered MR-damper-based vibration control systems and new applications have been designed. For example, Cho *et al* (2004) presented an MR damper with the EMI for a civil engineering application and showed that the performance of this system is comparable to that of conventional MR-damper-based systems. Cho *et al* (2005) described a conceptual design of the EMI in a self-powered MR-damper-based vibration reduction system and proposed its application for large-scale civil structures. Also Cho *et al* (2007) demonstrated the structure of the EMI to be used with the MR damper. Hong *et al* (2005) verified the efficiency of a smart passive system based on the MR damper and the EMI through experiments applying various historical earthquakes. Also Hong *et al* (2007) presented a smart MR-damper-based passive system with the EMI to verify the effectiveness for seismic protection of highway bridge. Jung *et al* (2004) described state-of-the-art semi-active control systems using MR dampers in civil engineering applications. Also Jung *et al* (2006) tested some control algorithms to verify the effectiveness of the MR-damper-based control system for seismic protection of the base isolation system and revealed that the system could be beneficial in reducing seismic response. Jung *et al* (2009a) investigated experimentally the sensing capability of the EMI that was incorporated in a vibration control system based on an MR damper and showed that the device may be considered as a velocity-sign sensor. Jung *et al* (2009b) investigated the design and performance verification of the MR-damper-based smart passive control system employing the EMI for the benchmark highway bridge model subjected to various historic earthquakes. Jung *et al* (2010a) verified experimentally the feasibility of an adaptive passive control system, which consists of the MR damper and the EMI for suppressing vibration of building structures subjected to ground accelerations and compared the performance of the system with that of passively operated MR-damper-based semi-active control systems. Also Jung *et al* (2010b) studied a sensing capability of the EMI system that was incorporated in the MR-damper-based vibration control system and showed that the EMI could act as a relative velocity sensor for common control methods for MR-damper-based systems. Wang *et al* (2009) studied a semi-active MR-damper-based vibration control system and system regeneration applied to an elevated highway bridge. Also Wang *et al* (2010) presented an integrated relative displacement self-sensing MR damper to realize the integrated relative displacement sensing and controllable damping.

This paper outlines the model and the structure of the proposed semi-active MR-damper-based vibration control system, and summarizes the selected results of experimental tests. The main objectives of the study were:

- to demonstrate that the system is feasible,
- to realize this system,
- to examine the performance of the system through experiments.

The system was examined when the control coil of the damper was voltage-supplied directly from the EMI or voltage-supplied via the rectifier, or supplied with a current control system with two feedback loops (the external loop with a sky-hook algorithm and the internal loop with the algorithm switching the photorelay, at the output from the rectifier). The results were compared with those obtained for the passive system (MR damper is off-state) and for the system with an external power source (EPS) when the control coil of the damper was supplied using a DC power supply and analogue voltage amplifier or a DC power supply and a photorelay.

The experiments were conducted in a specially engineered experimental set-up which incorporated the vibration generation system, the vibration control system (the EMI and the MR damper) with a spring attached, a movable platform (body), and the measurement–control system. The platform and the spring comprises a single DOF mechanical system. This system was designed to imitate the simple model of the first floor in the structure acting as the insulating base protecting the entire structure from the effects of undesired vibrations.

2. Model of the MR-damper-based vibration control system

The MR-damper-based vibration control system is an electro-mechanical system that comprises two interconnected

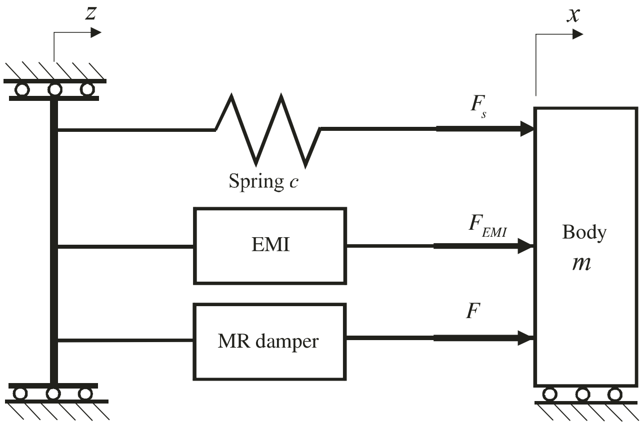

Figure 2. Schematic diagram of the mechanical subsystem.

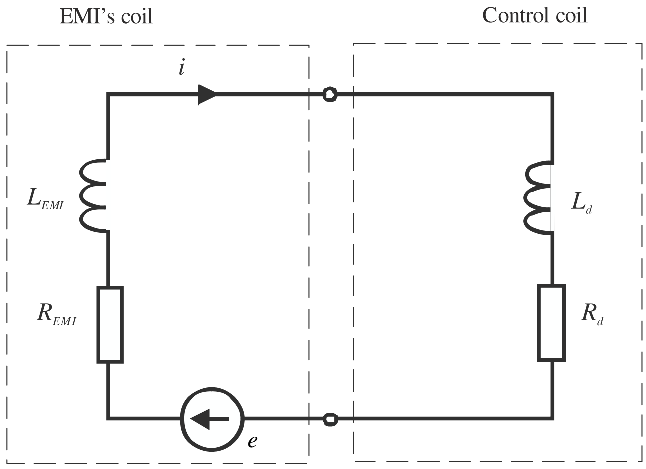

Figure 3. Schematic diagram of the electrical subsystem.

subsystems depicted schematically in figures 2 and 3. The diagram of the mechanical subsystem shows its main components and applied excitation (displacement)—z, the body displacement—x, the acting force of the EMI—F_{EMI}, the damper force—F, and the force of a spring acting upon the body—F_{s}. The forces F_{EMI}, F, and F_{s} act upon the body of mass m. The diagram of the electrical subsystem comprises the connected EMI's coil and the MR damper control coil. R_{EMI} and L_{EMI} denote the resistance and inductance of the EMI's coil, R_{d} and L_{d} are the resistance and inductance of the MR damper's coil whilst e denotes electromotive force (emf) and i current in the EMI–MR-damper circuit.

The motion of the mechanical subsystem is governed by the equation:

$$m\ddot{x} = c(z - x) + F_{\mathrm{EMI}} + F \tag{1}$$

where c is the stiffness factor of a spring.

Recalling Faraday's law and assuming that the magnetic field is distributed uniformly with cylindrical symmetry (assuming the magnetic field distribution to be uniform and displaying cylindrical symmetry) the emf induced by the magnets' motion with respect to the EMI's coil windings is given by the formula:

$$e = k(\dot{z} - \dot{x}) \tag{2}$$

where k is the EMI's constant associated with the number of turns per the coil's unit length and with the properties of the magnets.

Recalling equation (2), the force of the EMI acting upon the body can be written as:

$$F_{\mathrm{EMI}} = ki. \tag{3}$$

According to Guo *et al* (2006), Kwok *et al* (2006), the force generated by the damper MR, whose sense depends on the sign of the relative velocity $(\dot{z} - \dot{x})$ is given by the formula:

$$\begin{aligned} F = {} & (c_1|i| + c_2)\tanh[\beta\,((\dot{z} - \dot{x}) + p_1(z - x))] \\ & + (c_3|i| + c_4)\,((\dot{z} - \dot{x}) + p_2\,(z - x)) \end{aligned} \tag{4}$$

where c_1, c_2, c_3, c_4 are constants in the MR damper model, and β, p_1, p_2, are scaling parameters enabling transition, in the pre-yield region, from negative to positive velocities.

The equation describing the electrical subsystem can be written as:

$$e - (R_{\mathrm{EMI}} + R_{\mathrm{d}})i - (L_{\mathrm{EMI}} + L_{\mathrm{d}})\frac{\mathrm{d}i}{\mathrm{d}t} = 0. \tag{5}$$

Assuming the following state variables: $y_1 = x$—body displacement, $y_2 = \dot{x}$—body velocity, $y_3 = i$—current in the EMI–MR-damper circuit, the mathematical model of the system becomes:

$$\begin{aligned} \dot{y}_1 &= y_2 \\ \dot{y}_2 &= \frac{1}{m}\{[c\,(z - y_1) + k\,y_3 + (c_1\,|y_3| + c_2) \\ &\quad \times \tanh[\beta\,((\dot{z} - y_2) + p_1\,(z - y_1))] \\ &\quad + (c_3\,|y_3| + c_4)\,((\dot{z} - y_2) + p_2\,(z - y_1))]\} \\ \dot{y}_3 &= \frac{1}{(L_{\mathrm{EMI}} + L_{\mathrm{d}})}[k\,(\dot{z} - y_2) - (R_{\mathrm{EMI}} + R_{\mathrm{d}})\,y_3]. \end{aligned} \tag{6}$$

The above model was used to study the feasibility of the proposed MR-damper-based vibration control system. The numerical simulation procedure assumed the following values of parameters: $m = 103$ kg, $c = 10^5$ N m^{-1}, $R_{\mathrm{d}} = 5.5\ \Omega$, $L_{\mathrm{d}} = 125$ mH, $R_{\mathrm{EMI}} = 0.25\ \Omega$, $L_{\mathrm{EMI}} = 4.78$ mH, $k = 30$ N A^{-1}, $c_1 = 970$ N A^{-1}, $c_2 = 50$ N, $c_3 = 3745$ N s A^{-1} m^{-1}, $c_4 = 322$ N s m^{-1}, and sine applied excitation z of amplitude 3.5 mm and frequency in the range 2–10 Hz. The parameters c_1, c_2, c_3, and c_4 of the RD-1005-3 damper model were determined in the identification procedure. For this purpose experiments were performed on a testing machine involving force measurements for the preset sine displacement excitations of amplitude 6 mm and frequency in the range 0.5–6.5 Hz that was varied every 0.5 Hz. Figure 4 shows predicted and measured force–velocity loops $F(v)$ of the damper achieved at frequency 4.5 Hz. It is apparent that the predicted loop agrees well with experimental data.

Selected results of simulations are shown in figures 5–7. Figure 5 presents time histories of the emf e produced by the

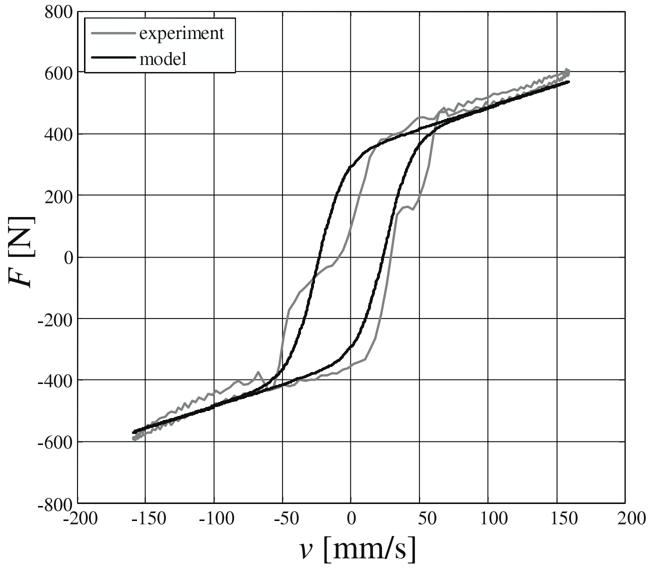

Figure 4. Predicted and measured force F versus piston velocity v of the damper for sine displacement excitation with amplitude 6 mm and frequency 4.5 Hz.

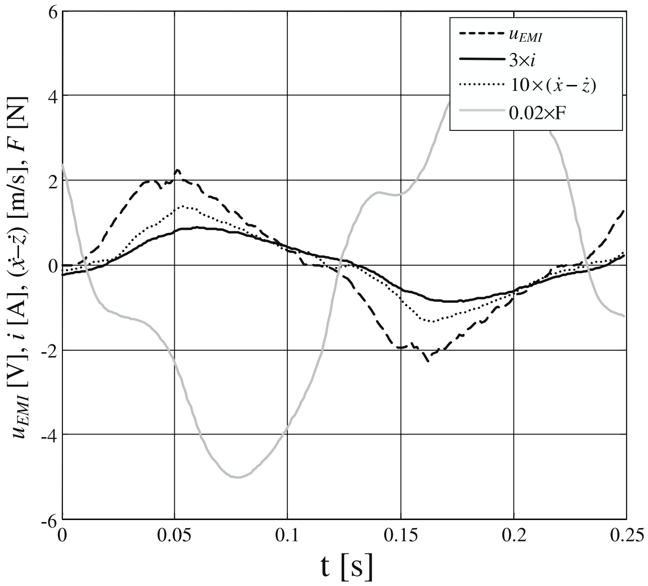

Figure 6. Predicted voltage u_{EMI} and current in the control coil i, relative velocity $(\dot{x} - \dot{z})$, and damper force F at frequency 4.5 Hz.

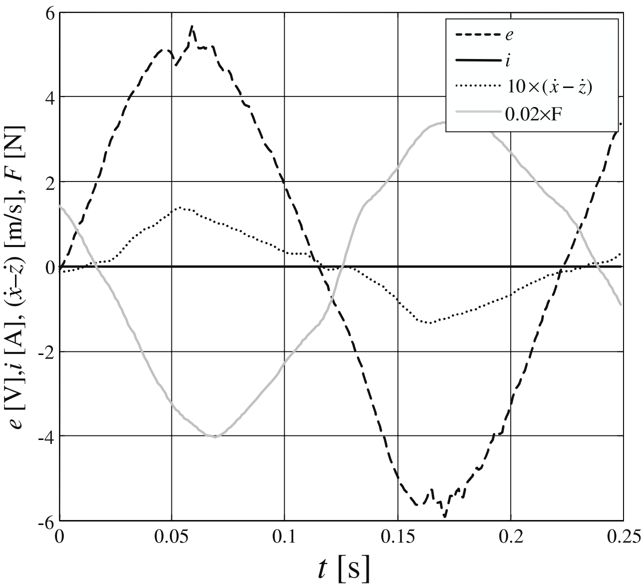

Figure 5. Predicted electromotive force e, current in the control coil i, relative velocity $(\dot{x} - \dot{z})$, and damper force F at frequency 4.5 Hz.

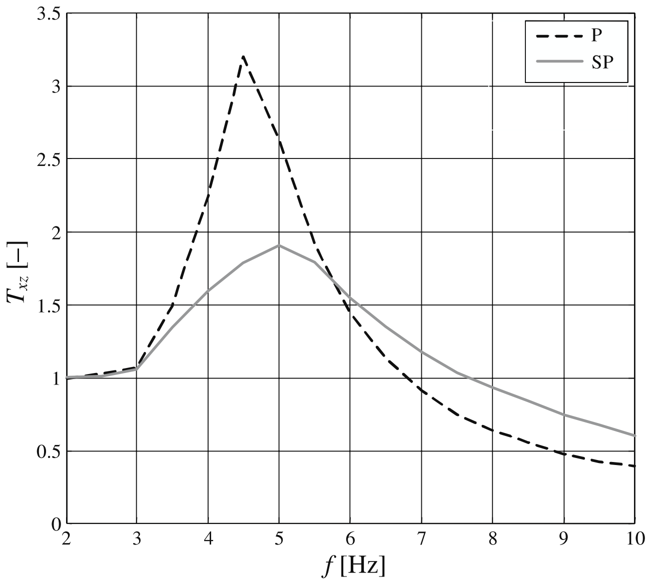

Figure 7. Predicted transmissibility coefficient T_{xz} versus frequency f for the systems P and SP.

generator, relative velocity $(\dot{x} - \dot{z})$, and damper force F in the case of the passive system (P)—with no current in the MR damper's coil. Figure 6 shows time histories of the voltage and current in the generator–MR-damper circuit, relative velocity $(\dot{x} - \dot{z})$ and damper force F in the case of a self-powered system (SP)—the MR damper' coil is power-supplied from the generator. The numerical data obtained for the system P revealed that the higher the frequency of z, the greater is the emf e produced. Similar to the SP, the higher the frequency of z, the greater voltage u_{EMI}, current i, and force F are obtained, and the phase shift of current with respect to voltage depends on the frequency of excitation z.

Figure 7 compares displacement transmissibility plots of P to SP systems. The resonance frequency of the system P is 4.5 Hz and the system SP is 5 Hz. It is clearly apparent that significant vibration reduction can be obtained in the near-resonance frequency range of the system P when compared to the system SP.

3. Structure of the engineered MR-damper-based vibration control system

The MR-damper-based vibration control system comprises the EMI engineered by the author (Sapiński 2010) and the damper RD-1005-3. The structure of the EMI is shown in figure 8.

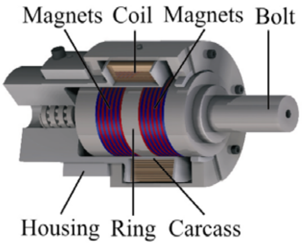

Figure 8. Structure of the EMI.

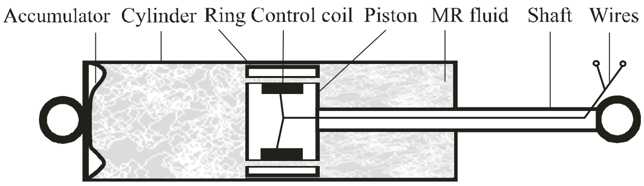

Figure 9. Structure of the MR damper.

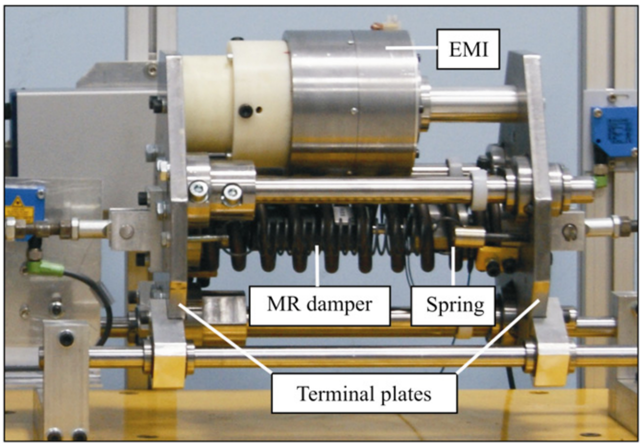

Figure 10. Structure of the MR-damper-based vibration control system.

The device is symmetrical and complete with two neodymium–boron magnet systems (six magnets in each). The magnets are ring-shaped, display axial magnetization, and are fixed on a bolt made from non-ferromagnetic material. The magnets in the system are arranged such that they face one another with opposite poles, but the magnets' systems are configured such that identical poles lie opposite to one another. In the space between the magnet systems is a ferromagnetic ring, and the coil winding, wound on a carcass with copper foil with one-sided insulation, incorporates 260 turns. The EMI is locked inside a housing made from ferromagnetic material. The resistance and the inductance of the EMI's coil are $R_{\mathrm{EMI}} = 0.25\ \Omega$ and $L_{\mathrm{EMI}} = 4.78$ mH.

The structure of the RD 1005-3 damper with main components is shown in figure 9. The technical specification of this damper is provided in Lord Technical Data (www.lord.com). The resistance and the inductance of the RD-1005-3 damper's coil are $R_{\mathrm{d}} = 5.5\ \Omega$ and $L_{\mathrm{d}} = 125$ mH.

Figure 10 shows the structure of the engineered vibration control system. A spring is connected in parallel to the EMI and to the damper RD-1005-3. These three components are fixed between two terminal plates and connected on one end to the shaker and to the platform on the other. Trolleys moving along the linear guides are attached to the platform, comprising three horizontally arranged plates. The trolleys enable the platform motion along the horizontal axis. The guides and the vibration reduction system are attached to the steel frame. Additionally, the system incorporates two springs (invisible in figure 10) to compensate for forces due to the presence of the accumulator in the damper RD-1005-3.

4. Experimental set-up

The schematic diagram of the experimental set-up, incorporating an electromagnetic shaker (LDS, model V780), a vibration reduction system (EMI and the damper RD-1005-3), a spring connected in parallel (rigidity 10^5 N m^{-1}), a mobile platform (mass 103 kg), two laser displacement sensors (Sensor 1, Sensor 2), two tensometric force sensors (Sensor 3), and the measurement and control system is shown in figure 11. Symbols P, SP, SP_r, SP_r_sh-d are associated with the investigated cases of power-supplying the coil. The measurement and control circuit incorporates a PC computer with the analogue-to-digital/digital-to-analogue (AD/DA) card supported by Windows XP, using the MATLAB/Simulink software. The recorded quantities include the displacement of the shaker core (excitation signal) z, platform displacement x, damper force F, output voltage in the generator (emf) $u(e)$, and current i in the control coil. Measured quantities are converted into voltage signals in the range $(-10, +10)$ V and sampled with a frequency of 1 kHz. The experimental set-up ready for tests is shown in figure 12.

5. Experiments

The aim of the experiments was to demonstrate the self-powered and sensing capabilities of the vibration control system. Excitations applied during the experimental programme were sine signals of amplitude 3.5 mm and frequency in the range 2–10 Hz that was varied every 0.25 Hz. The characteristics of the vibration control system with energy harvesting are then compared with those of a conventional semi-active system with an external power source.

First, the performance of each system was investigated through obtaining the time patterns of selected quantities. These characteristics are collected for the resonance frequency of the system $f_0 = 4.5$ Hz. The relationship is found between the current in the control coil, the damper force, and frequency, utilizing the average rectified values of these quantities derived from the formulae:

$$I = \frac{1}{T}\int_t^{t+T} |i(\tau)|\,\mathrm{d}\tau, \qquad F = \frac{1}{T}\int_t^{t+T} |F(\tau)|\,\mathrm{d}\tau \quad (7)$$

where T denotes the period of measured quantities $i(t)$ and $F(t)$.

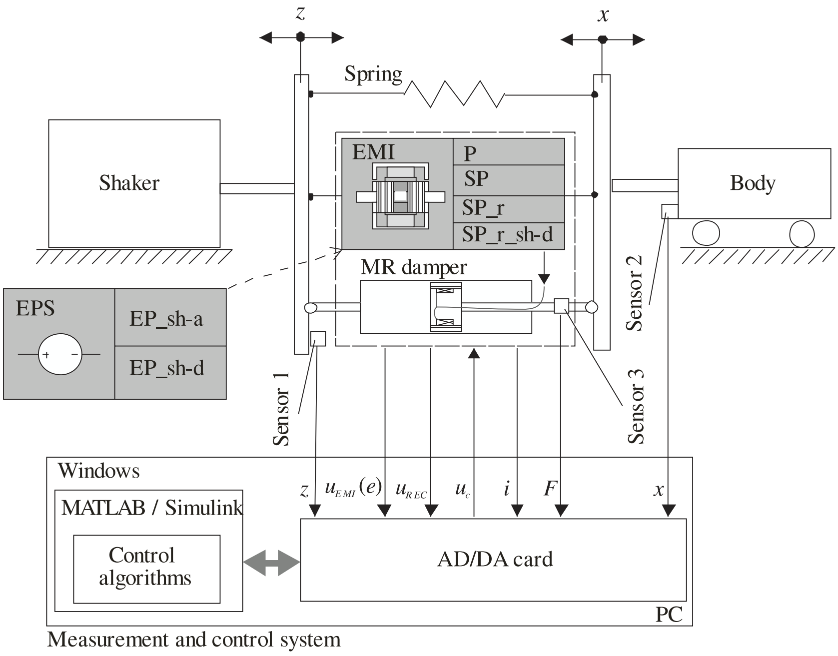

Figure 11. Schematic diagram of the experimental set-up.

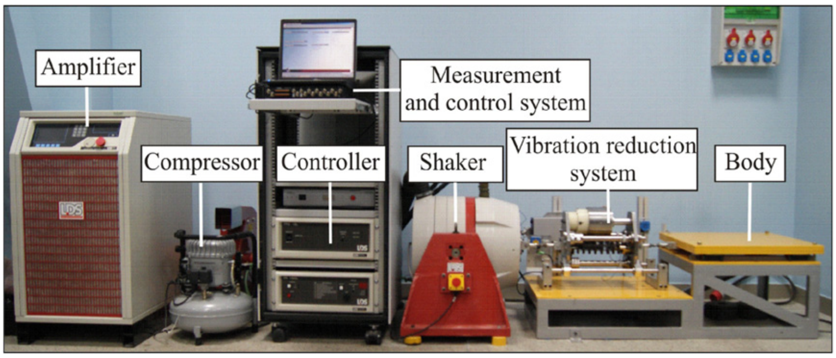

Figure 12. View of the experimental set-up.

The transmissibility coefficient was calculated for each frequency in the range 2–10 Hz from the formula:

$$T_{xz} = \frac{\dot{X}}{\dot{Z}} = \frac{\frac{1}{T}\int_t^{t+T} |\dot{x}(\tau)|\,\mathrm{d}\tau}{\frac{1}{T}\int_t^{t+T} |\dot{z}(\tau)|\,\mathrm{d}\tau} \tag{8}$$

where $\dot{x}(t)$ is the platform velocity, $\dot{z}(t)$ is the shaker core velocity and $\dot{X}$, $\dot{Z}$ are the average values of these quantities.

5.1. System with energy harvesting

The operation of the system with energy harvesting is investigated and in the cases considered here the control coil:

- was not supplied with current (system P),
- was supplied directly with the voltage u_{EMI} generated by the EMI (system SP),
- was supplied directly with voltage generated by the EMI and rectified u_{REC} (system SP_r),
- was supplied with current controlled by the analogue relay placed on the output from the rectifier–Graetz-bridge (system SP_r_sh-d).

As regards the system P, there is no connection between the control coil and the coil in the generator ($i = 0$ A, MR damper in the off-state), hence we get a passive system (figure 13). Time patterns of electromotive force induced in the generator (emf) e, relative velocity $(\dot{x} - \dot{z})$, current in the control coil i, and damper force F in the system P are shown in figure 14. It is apparent that the emf pattern resembles that of the relative velocity.

In the system SP the control coil is directly supplied with voltage u_{EMI} from the EMI, hence we get a self-powered system (figure 15). Time patterns of u_{EMI}, of current in the control coil, relative velocity $(\dot{x} - \dot{z})$, and damper force F in the system SP are shown in figure 16. It is apparent that the voltage and current patterns resemble that of relative velocity. The phase shift between the voltage and current equals $\varphi = 34°$ and varies depending on the frequency of the applied excitation z.

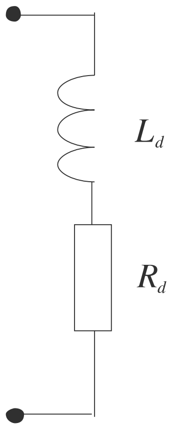

Figure 13. Control coil with no power-supply.

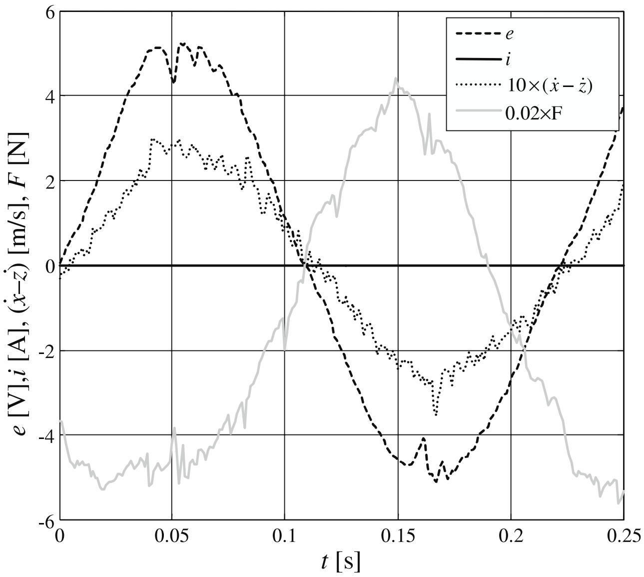

Figure 14. Electromotive force e, current in the control coil i, relative velocity $(\dot{x} - \dot{z})$, and damper force F at frequency 4.5 Hz.

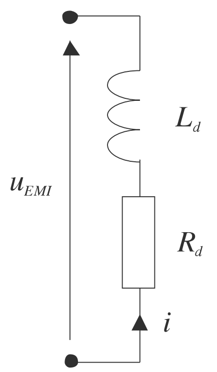

Figure 15. Control coil supplied by the EMI.

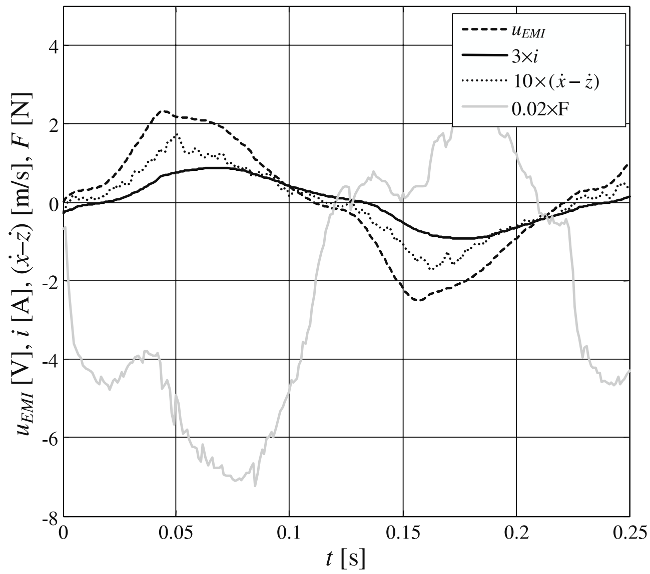

Figure 16. Voltage u_{EMI} and current in the control coil i, relative velocity $(\dot{x} - \dot{z})$, and damper force F at frequency 4.5 Hz.

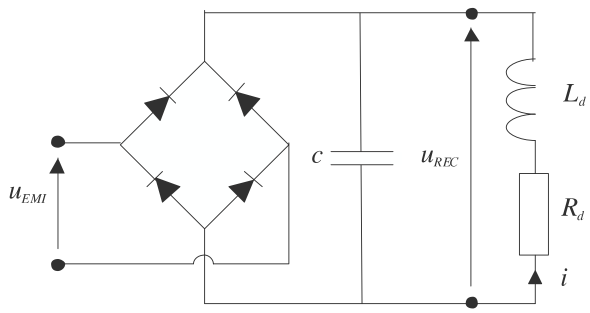

Figure 17. Control coil supplied by the EMI with a rectifier.

In the system SP_r, the control coil is supplied with output voltage from the rectifier (Graetz bridge) u_{REC} (figure 17). On the output from the bridge, incorporating Schottky diodes of the type STPS2L40U, (http://www.st.com), is a condenser with the capacitance $C = 4.7$ mF. Time patterns of voltage u_{REC} and current i in the control coil, of relative velocity $(\dot{x} - \dot{z})$ and damper force F in the system SP_r are shown in figure 18. It appears that voltage and current patterns follow that of relative velocity. The delay of the current intensity pattern with respect to voltage u_{REC} is apparent, too.

In the system SP_r_sh-d, current in the control coil was controlled by a photoMOS relay of the type AQY211EH (http://www.panasonic-electric-works.com/catalogues) connected to the Graetz bridge (figure 19). It is worthwhile mentioning that in this configuration the condenser C is behind the photoMOS relay and the control of current uses two feedback loops, the external and internal ones. In the external loop a sky-hook control algorithm is implemented (Braun *et al* 2002), given as:

$$i_{\mathrm{sky}} = \begin{cases} b_i \cdot |\dot{x}|\,, & \dot{x}(\dot{x} - \dot{z}) \geqslant 0 \\ 0, & \dot{x}(\dot{x} - \dot{z}) < 0 \end{cases} \tag{9}$$

where the proportionality factor $b_i = 0.002$ A s mm^{-1} was selected empirically.

In the internal loop a photorelay is realized whose function is to maintain the current i_{sky} on the level determined by the sky-hook control algorithm. Based on the error signal (i_{sky} −

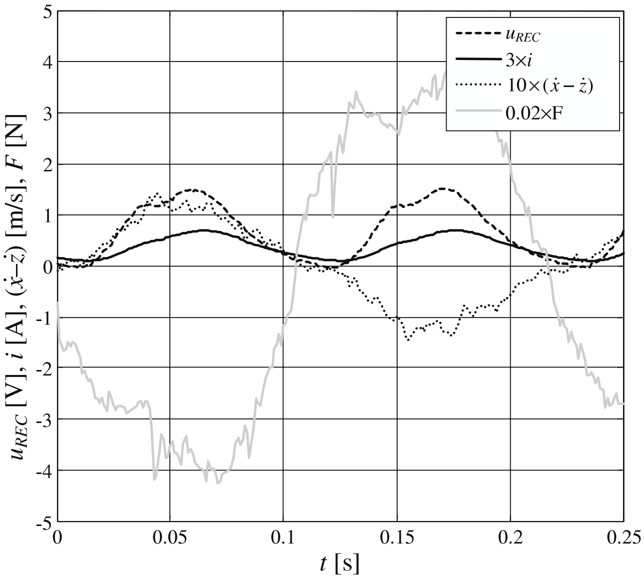

Figure 18. Voltage u_{REC}, current in the control coil i, relative velocity $(\dot{x} - \dot{z})$ and damper force F at frequency 4.5 Hz.

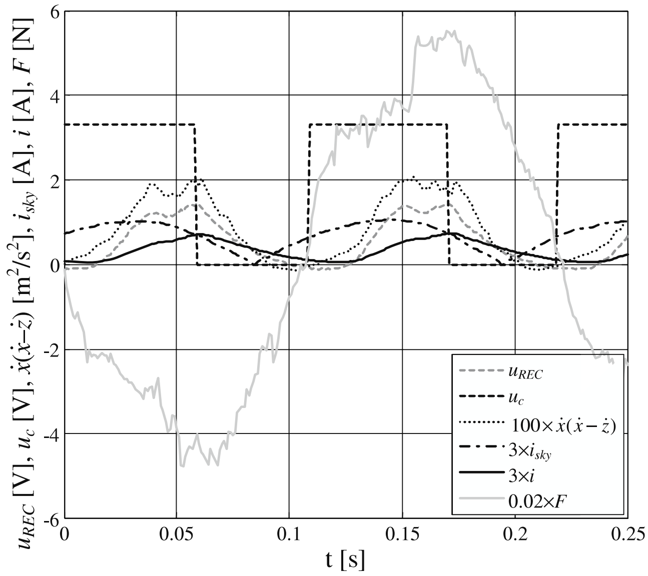

Figure 20. Voltage u_{REC}, control voltage u_{c}, velocity product $\dot{x}(\dot{x} - \dot{z})$, current i_{sky}, current in the control coil i, and damper force F at frequency 4.5 Hz.

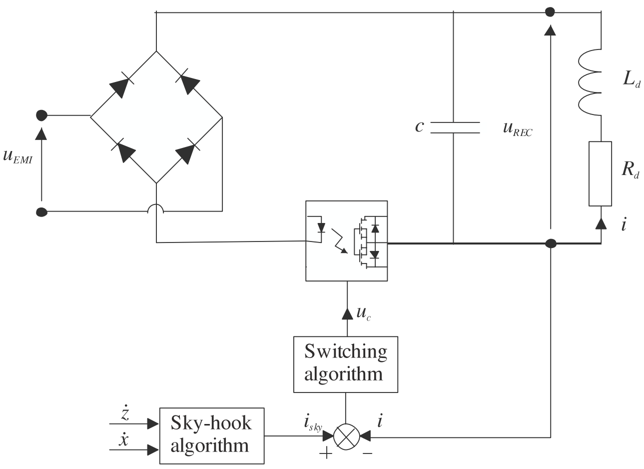

Figure 19. Control coil supplied by the EMI with rectifier and photorelay.

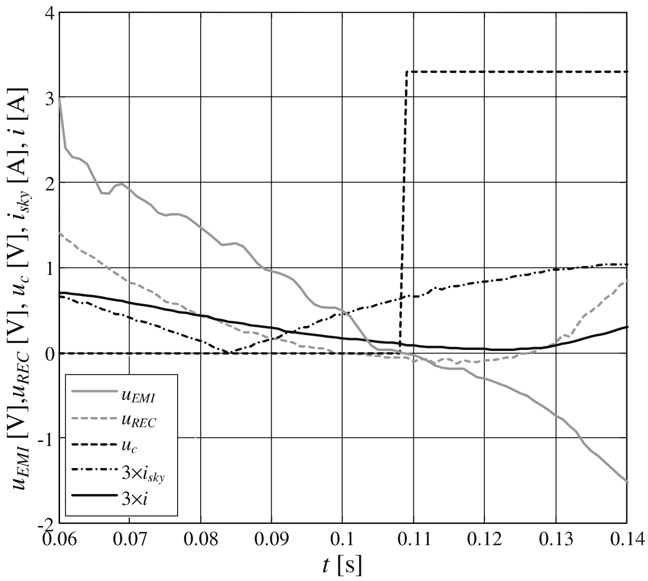

Figure 21. Enlarged section of voltage u_{REC} and u_{EMI}, control voltage u_{c}, current i_{sky}, current in the control coil i at frequency 4.5 Hz.

i), the switching algorithm determines the command signal (voltage signal) u_{c}, which can assume two values: $u_{\mathrm{ch}} = 3.3$ V (the photorelay is on) or $u_{\mathrm{cl}} = 0$ V (the photorelay is off). This algorithm can be expressed by the formula:

$$u_{\mathrm{c}} = \begin{cases} u_{\mathrm{ch}}, & i < i_{\mathrm{sky}} \\ u_{\mathrm{cl}}, & i \geqslant i_{\mathrm{sky}}. \end{cases} \tag{10}$$

Time patterns of rectified voltage u_{REC}, of voltage controlling the photorelay u_{c}, the product of velocity $\dot{x}(\dot{x} - \dot{z})$, current i, and i_{sky}, and damper force F in the system SP_r_sh-d are shown in figure 20. Figure 21 shows the enlarged section of the system operation during the time interval when the photorelay is switched. Plots in figure 20 reveal that for $\dot{x}(\dot{x} - \dot{z}) \geqslant 0$ the current i_{sky} is generated, its value proportional to the velocity $|\dot{x}|$. When $i_{\mathrm{sky}} = 0$ A, the current intensity i will not assume the value 0 A, on account of the electric charge accumulated in the condenser C. When the photorelay is off ($u_{\mathrm{c}} = u_{\mathrm{cl}}$), the voltage u_{REC} decreases, assuming negative values in the time interval (0.1, 0.125) s (see figure 21). At the same time the coil controlling the damper is power-supplied by the charged condenser C. When the photorelay is switched on ($u_{\mathrm{c}} = u_{\mathrm{ch}}$), the voltage u_{REC} begins to increase after about 20 ms, due to the fact that at the instant the photorelay is switched on, the voltage $u_{\mathrm{EMI}} < 0.65$ V. Repeated charging of the condenser C begins at the time instant when $u_{\mathrm{EMI}} > 0.65$ V (the voltage assumes a value higher than the voltage decrease across the Schottky diodes).

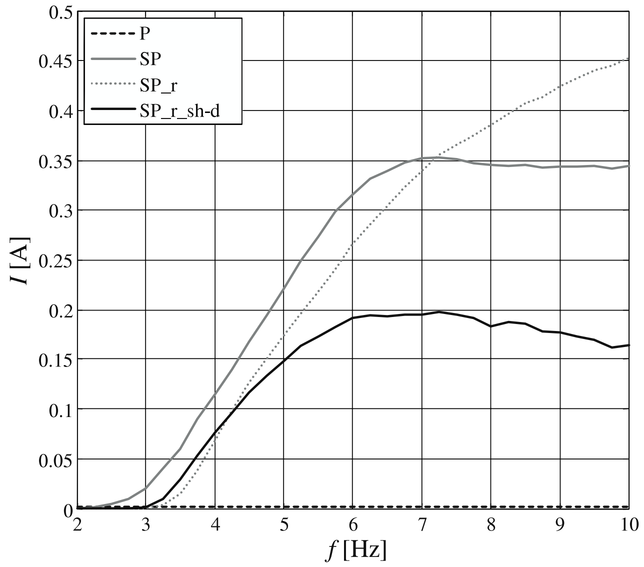

Figure 22. Current in the control coil i versus frequency f for the systems: P, SP, SP_r, SP_r_sh-d.

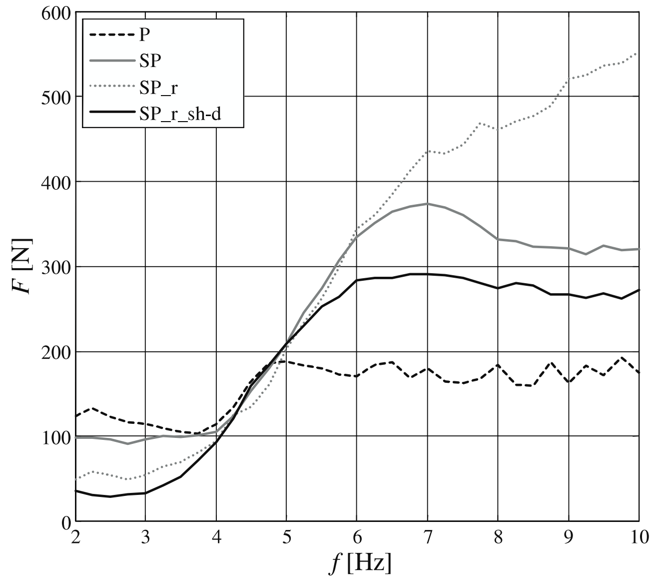

Figure 23. Damper force F versus frequency f for the systems: P, SP, SP_r, SP_r_sh-d.

Time patterns of the registered quantities reveal the self-powered capability of the systems SP, SP_r, and SP_r_sh-d.

Figures 22 and 23 show the plots of average rectified values of current in the control coil and damper force as a function of frequency ($I(f)$, $F(f)$) for the systems P, SP, SP_r, and SP_r_sh-d. Figure 22 reveals that in the systems SP and SP_r the current I increases with the excitation frequency f, which leads to the increase of the damper force F (figure 23). Plots in figure 24, showing the transmissibility coefficient $T_{xz}(f)$, demonstrate that the system SP_r_sh-d exhibits most favourable features, even though for the frequency $f > 6$ Hz the coefficient T_{xz} tends to be higher than in the system P. Although at the resonance frequency both the systems SP and SP_r feature the lower transmissibility coefficient T_{xz} in relation to P; the most disadvantageous aspect of the system SP is that T_{xz} tends to increase for the frequency $f > 5.5$ Hz, and for frequencies $f > 6$ Hz (SP_r).

5.2. System using an external power source

The performance of the system with an external power source (a conventional system) was investigated and in the cases considered here the control coil was power-supplied by:

- an EPS DC power supply and analogue voltage amplifier (system EP_sh-a),
- an EPS DC power supply and photorelay (system EP_sh-d).

These configurations are shown schematically in figure 11, in which the EMI block is replaced by an EPS block. It is worthwhile mentioning that in the system EP_sh-d the photorelay is supplied from the DC power supply amplifier whilst in the system SP_r_sh-d the photorelay is powered by the EMI.

In the system EP_sh-a the analogue voltage amplifier generates a voltage associated with the control voltage u_{sky}.

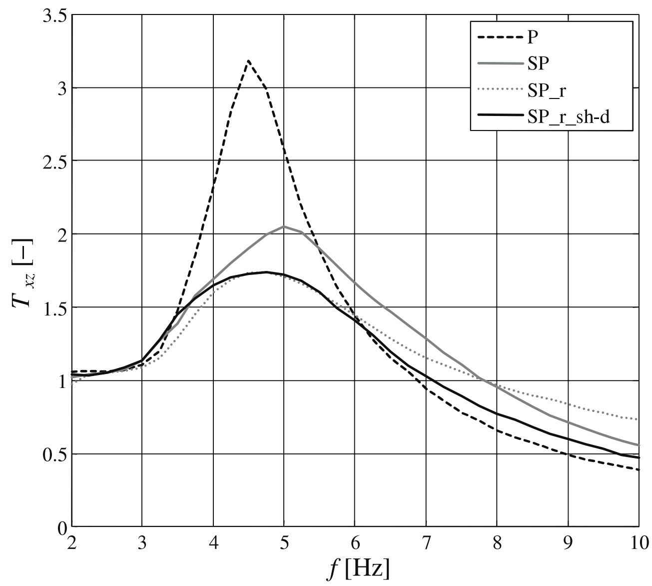

Figure 24. Transmissibility coefficient T_{xz} versus frequency f for the systems: P, SP, SP_r, SP_r_sh-d.

This voltage is generated by the sky-hook algorithm activated on a PC with a card AD/DA-model RT-DAC 4 (http://www.inteco.com.pl). In both cases the generator coil is connected only to the measurement circuit (no loading) and the emf force is utilized in monitoring of the relative velocity $(\dot{x} - \dot{z})$. One has to bear in mind that the control voltage u_{c} in the system EP_sh-d becomes an on/off signal, whilst in the EP_sh-a it becomes an analogue signal in the range 0–10 V (figure 25). In both systems the control of current in the control coil is implemented using a sky-hook algorithm. Like in the system SP_r_sh-d, we get two feedback loops (figure 19).

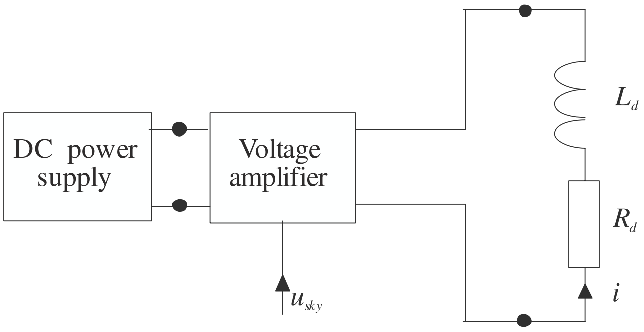

Figure 25. Control coil supplied by a DC power supply and voltage amplifier.

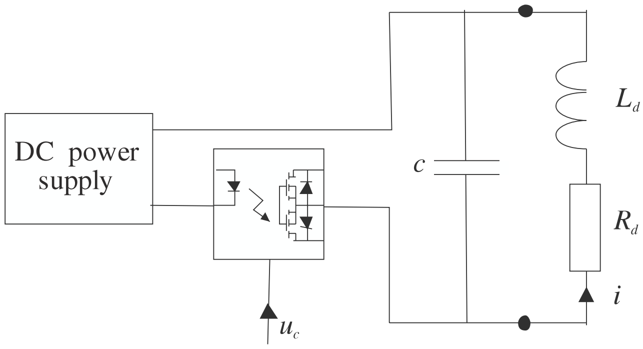

Figure 27. Control coil supplied by a DC power supply and photorelay.

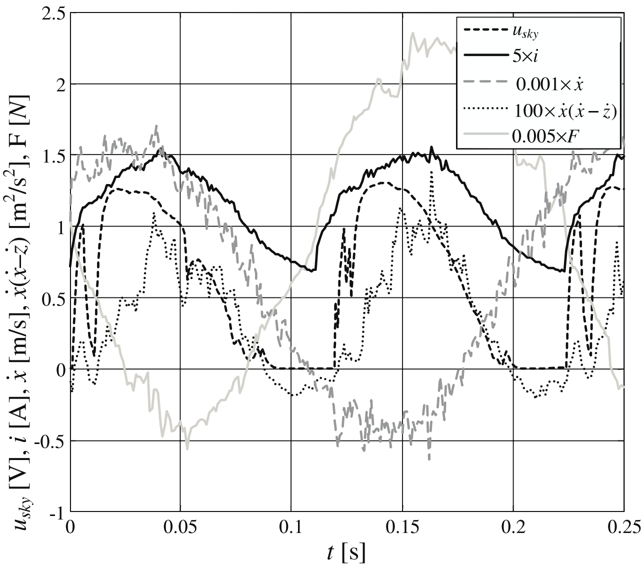

Figure 26. Voltage u_{sky}, current in the control coil i, velocity $\dot{x}$, velocity product $\dot{x}(\dot{x}-\dot{z})$, and damper force F at frequency 4.5 Hz.

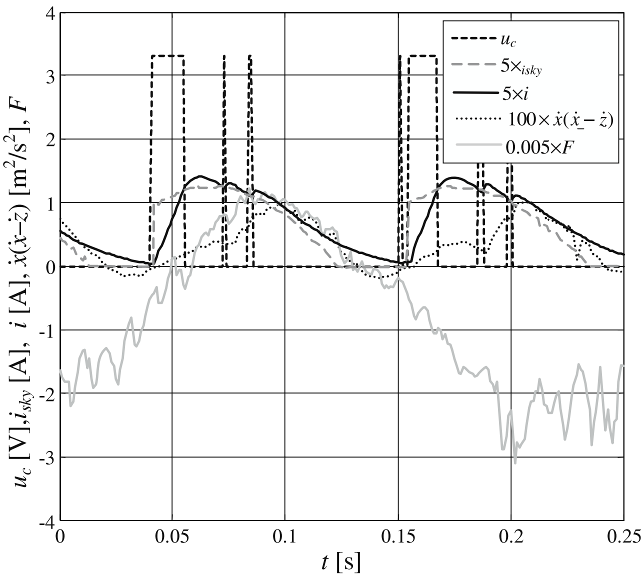

Figure 28. Voltage u_{c}, current i_{sky}, current in the control coil i, velocity product $\dot{x}(\dot{x}-\dot{z})$ and damper force F at frequency 4.5 Hz.

The voltage amplifier in the system EP_sh-a generates the command signal u_{sky} in accordance with the formula:

$$u_{\text{sky}} = \begin{cases} b_u \cdot |\dot{x}|, & \dot{x}(\dot{x}-\dot{z}) \geqslant 0 \\ 0, & \dot{x}(\dot{x}-\dot{z}) < 0. \end{cases} \tag{11}$$

The value of the coefficient $b_u = 0.01$ V s mm^{-1} is selected taking into account the coefficient b_i (equation (9)) and resistance of the control coil in the damper R_{d}.

Time patterns of the control voltage u_{sky}, current i in the control coil, the product of velocity $\dot{x}(\dot{x}-\dot{z})$, and the damper force F are shown in figure 26. It is apparent that in the time intervals when $\dot{x}(\dot{x}-\dot{z}) < 0$ the signal $u_{\text{sky}} = 0$, and when $\dot{x}(\dot{x}-\dot{z}) \geqslant 0$, then $u_{\text{sky}} = 0.01|\dot{x}|$.

In the system EP_sh-d, the current in the control coil is controlled by the photorelay through the voltage u_{c} (figure 27). Time patterns of the control voltage u_{sky}, current i_{sky}, and current i in the control coil, the product of velocity $\dot{x}(\dot{x}-\dot{z})$ and the damper force F are shown in figure 28. The plots indicate that the photorelay is not on when $\dot{x}(\dot{x}-\dot{z}) < 0$. When the photorelay is triggered on by the signal u_{c}, the current intensity i increases after about 2 ms (the duration of photorelay activation). In the time intervals when the current intensity in the coil $i > i_{\text{sky}}$, the photorelay is switched off and then the condenser C begins to be discharged by the control coil.

Time patterns of parameters registered in the systems EP_sh-a and EP_sh-d demonstrate the good performance of those systems.

Figures 29 and 30 compare the characteristics $I(f)$, $F(f)$, $T_{xz}(f)$ of the vibration reduction systems with energy harvesting SP, SP_r_sh-d and of those with the external power supply: EP_sh-a and EP_sh-d. Plots in figure 29 reveal that in the systems EP_sh-a and EP_sh-d as well as SP_r_sh-d, the control of current in the control coil leads to the reduction of the damper force, which is not possible in the case of the system SP (figure 30). Plots of $T_{xz}(f)$ in figure 31 show that the most favourable behaviour in the frequency range 2–10 Hz is displayed by the systems EP_sh-a and EP_sh-d. Throughout this frequency range the coefficient T_{xz} will assume the smallest value. The system EP_sh-d appears

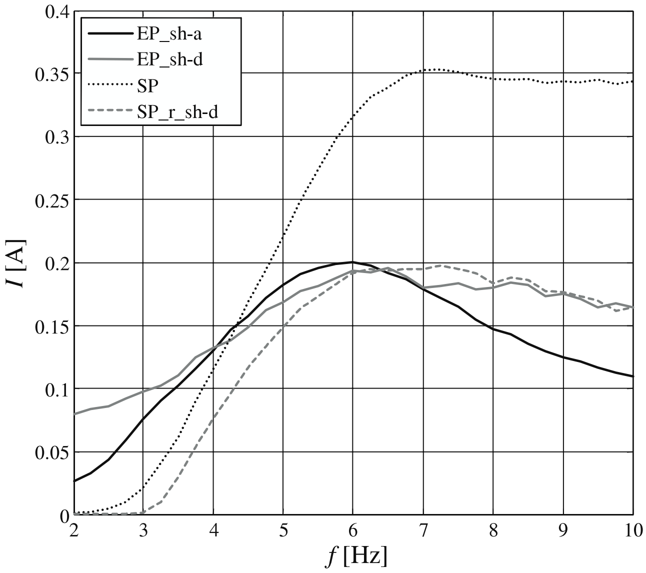

Figure 29. Current in the control coil I versus frequency for the systems: EP_sh-a, EP_sh-d, SP, SP_r_sh-d.

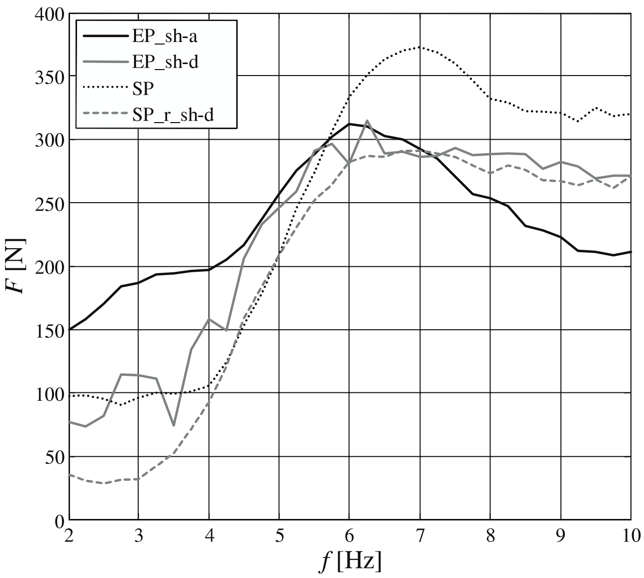

Figure 30. Damper force F versus frequency f for the systems: EP_sh-a, EP_sh-d, SP, SP_r_sh-d.

to perform better in the frequency range 3–7 Hz, whilst the system EP_sh-a—in the range $f > 7$ Hz.

The plots of voltage induced by the EMI and of the relative velocity in the system SP reveal a good agreement between the signs of these quantities, particularly the velocity $(\dot{x} - \dot{z}) > 0.2$ m s^{-1}. That confirms the suggestion put forward in Jung *et al* (2009a, 2009b), Wang *et al* (2010) that the EMI can be used as a 'relative velocity sensor' for the MR-damper-based semi-active vibration control system.

The investigation of the relationship between the relative velocity across the MR damper and the induced voltage from EMI by comparing their peak amplitude (peak relative velocity versus peak induced voltage) conducted by Jung *et al* (2009a, 2009b) indicated that the trend line of the data points is linear, demonstrating that the induced voltage signal is linearly proportional to the velocity signal. Accordingly, the relationship between the signal e (voltage u_{EMI}) and the signal $(\dot{x} - \dot{z})$ in the considered MR-damper-based vibration control system can be written as:

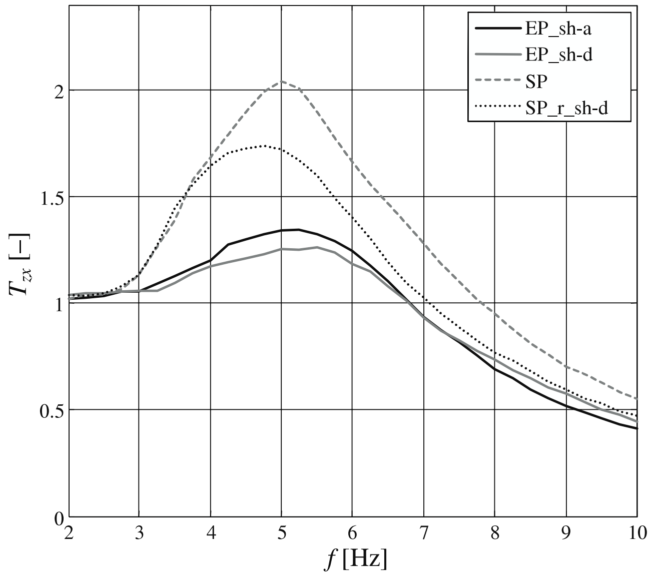

Figure 31. Transmissibility coefficient T_{xz} versus frequency f for the systems: EP_sh-a, EP_sh-d, SP, SP_r_sh-d.

Table 1. Identified coefficients κ and σ.

Frequency f (Hz)	Coefficient κ (V s m^{-1})	Coefficient σ (V)
3.0	9.50	0.0101
4.5	18.60	0.0113
6.0	18.20	0.0165
7.5	18.00	0.0170
9.0	17.70	0.0058

$$e = \kappa(\dot{x} - \dot{z}) + \sigma \tag{12}$$

where κ denotes a directional coefficient and s the shift coefficient of voltage.

In order that the EMI should provide the measurement data about the $(\dot{x} - \dot{z})$ velocity, the parameters κ and σ have to be first identified. For that purpose the identification experiments were conducted, which consisted in applying harmonic inputs z with amplitude 3.5 mm and frequencies in the range 2–10 Hz, that was varied every 0.25 Hz. Coefficients κ and σ were identified based on measured emf data e and relative velocity $(\dot{x} - \dot{z})$ for the applied excitation frequencies (2, 10) Hz for the system P. The identification procedure uses the function polyfit.m available in MATLAB. The values of the thus identified coefficients κ and σ for selected frequencies are summarized in table 1.

It appears that in the frequency range 4.5–7.5 Hz the values of κ will only slightly differ, whereas beyond this range the discrepancies are more significant. That is why the value of κ in further considerations is derived from equation (12), as the arithmetic mean of this coefficient obtained in the frequency

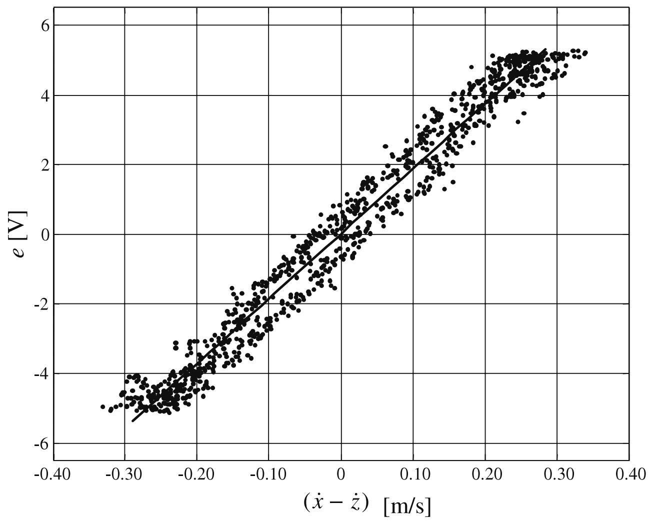

Figure 32. Electromotive force e versus relative velocity $(\dot{x} - \dot{z})$ for the system P at frequency 4.5 Hz.

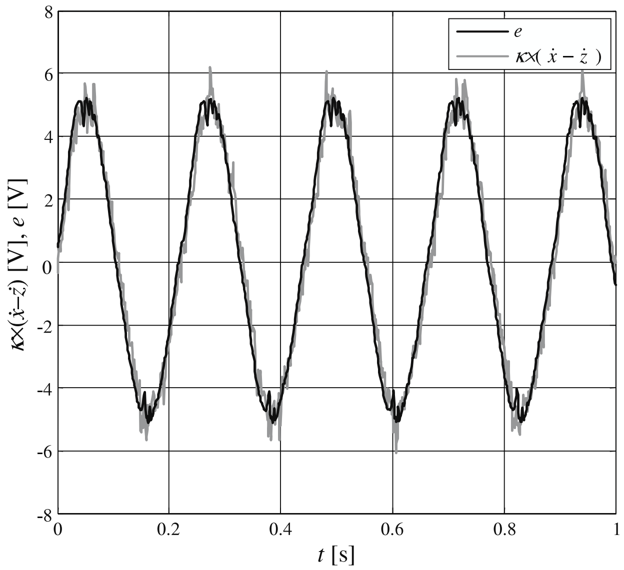

Figure 33. Time patterns of electromotive force e and product of relative velocity $(\dot{x} - \dot{z})$ and coefficient k for the system P at frequency 4.5 Hz.

range 4.5–7.5 Hz, yielding $\kappa = 18.27$ V s m^{-1}. As the values of σ are very small, it is assumed that $\sigma = 0$ V.

For those values of κ and σ, figure 32 shows the approximated relationship between emf and the relative velocity $(\dot{x} - \dot{z})$ (continuous line) against the measurement data (dotted lines). Figure 33 compares the registered pattern of emf force e and that of the product of relative velocity $(\dot{x} - \dot{z})$ and coefficient k in the system P under the applied excitation z of frequency 4.5 Hz. The plots in figure 33 reveal a good correspondence between those quantities.

Figure 34 shows the relationship between the average rectified value of the electromotive force E, relative velocity $(\dot{X} - \dot{Z})$, and frequency f. Particularly in the frequency range (2, 3.5) Hz, using the parameter E to compute $(\dot{X} - \dot{Z})$ Hz involves a significant error, due to low relative velocity levels 0.02–0.03 m s^{-1} corresponding to the emf values of $E < 0.5$ V.

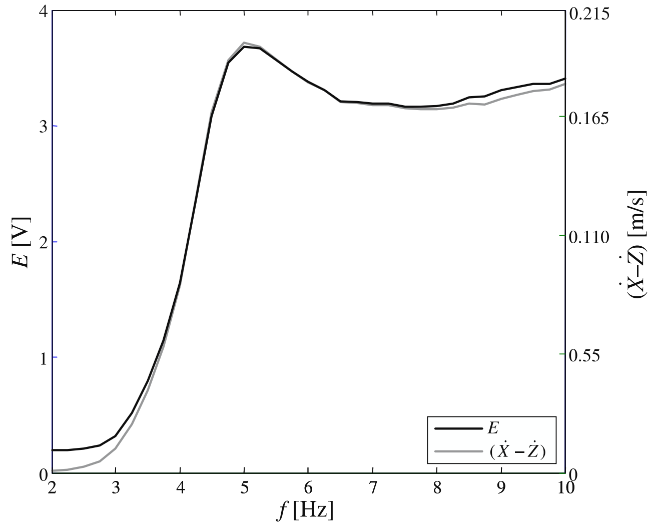

Figure 34. Electromotive force E versus frequency f for the system P.

6. Summary

The paper presents the structure, the model, and experimental investigation of the semi-active MR-damper-based vibration control system with energy harvesting, and summarizes the results of experiments. The system, comprising the EMI prototype and the damper RD 1005-3, employs an electromagnetic transduction mechanism to extract energy from vibrations. The experiments demonstrated that the proposed system is able to power-supply the MR damper and the EMI can act as a 'velocity-sign' sensor.

Among the tested systems with energy harvesting, the best performance in the near-resonance frequency range 3–6 Hz is offered by that referred to as SP_r_sh-d. However, the main drawback of this system is that the transmissibility coefficient tends to increase for frequencies higher than 6 Hz in relation to the system P. It appears that in this frequency range the energy extracted should be utilized to power-supply the control coil in the MR damper. It is observed that in the nearly whole frequency range the systems EP_sh-a and EP_sh-d offer better performance than SP_r_sh-d, yet those systems require an external power supply. The experiments conducted for the SP system revealed that the voltage signal from EMI agrees well with that of the relative velocity signal across the damper, in particular in the range 4.5–7.5 Hz. That is why this signal is able to provide the required measurement data and the EMI can well act as a 'velocity-sign sensor'. Therefore, only one displacement (accelerometer) sensor is needed to monitor absolute velocity of the body. This characteristic may be more useful for other control algorithms (e.g. clipped optimal or maximum energy dissipation) than the sky-hook algorithm used in the study. Such algorithms only require the sign change of the velocity signal rather than the exact magnitude and phase of the velocity signal.

It should be noted that because of constraints present in the experimental set-up, the MR damper interacts both with the shaker and the body (platform), and the dynamics of the MR damper is an integral part of the dynamic behaviour of the entire system. Besides, the parameters of the shaker restrict the range of amplitudes of the applied excitation. These problems, as well as parameters of the EMI and the MR damper, limit the testing capabilities and present certain difficulties while investigating the factors that impact on the dynamic characteristics of the control system and the effect of displacement amplitude at the present stage of the study.

Research is now being carried out to test the developed vibration control system, where the control coil in the MR damper is supplied from the EMI via a photorelay. The aim of these tests is to compare the system performance using the control algorithms mentioned previously. Research is also underway to improve the efficiency of the engineered energy extractor.

Acknowledgment

This research is supported by the State Committee for Scientific Research under grant no. N501 366934.

References

Braun S, Ewins D and Rao S S 2002 *Encyclopedia of Vibration* (*Active Control of Vehicle Vibration*) vol 1, ed M Ahmadian (New York: Academic) pp 37–45

Cho S W, Jung H J and Lee I W 2005 Smart passive system based on a magnetorheological dampers *Smart Mater. Struct.* **1** 707–14

Cho S W, Jung H J and Lee I W 2007 Feasibility study of smart passive control system equipped with electromagnetic induction device *Smart Mater. Struct.* **16** 2323–9

Cho S W, Park K S, Kim Ch H and Lee I W 2004 Smart passive system based on MR damper *1st Int. Conf. 'From Scientific Computing to Computational Engineering' (Athens)*

Guo S, Yang S and Pan C 2006 Dynamic modeling of magnetorheological damper behaviours *J. Intell. Mater. Syst. Struct.* **17** 3–14

Hong J H, Choi K M, Lee J H, Oh J W and Lee I W 2005 Experimental study on smart passive system based on MR damper *Proc. 18th KKCNN Symp. on Civil Engineering (Taiwan)*

Hong J H, Choi K M, Lee J H, Oh J W and Lee I W 2007 Application of smart passive damping systems using MR dampers to highway bridge structure *J. Mech. Sci. Technol.* **21** 844–983

Jung H J, Jang D D, Cho S W and Koo J H 2009a Experimental verification of sensing capability of an electromagnetic induction system for an MR fluid damper based control system *11th Conf. on Electrorheological Fluids and Magnetorheological Suspensions*; *J. Phys.: Conf. Ser.* **149** 012058

Jung H J, Jang D D, Choi K M and Cho S W 2009b Vibration mitigation of isolated highway isolated bridge using MR damper-based smart passive control system employing an electromagnetic induction part *Struct. Health Monit.* **16** 613–25 Special issue: Part 2: Benchmark Structural Control Problem for Seismically Excited Highway Bridge

Jung H J, Jang D D, Koo J H and Cho S W 2010b Experimental evaluation of a 'self-sensing capability of an electromagnetic induction system designed for MR dampers *J. Intell. Mater. Syst. Struct.* **21** 837–6

Jung H J, Jang D D, Lee H J, Lee I W and Cho S W 2010a Feasibility test of adaptive passive control system using mr fluid damper with electromagnetic induction part *J. Eng. Mech.* **136** 254–9

Jung H J, Lee I W, Lee H J and Spencer B F Jr 2006 MR damper-based semi-active control systems for a base isolated structure *Proc. 8th Int. Conf. on Motion and Vibration Control* pp 616–21

Jung H J, Spencer B F Jr, Ni Y Q and Lee I W 2004 State-of-the-art of semi-active control systems using MR fluid dampers in civil engineering applications *Struct. Eng. Mech.* **17** 493–526

Kwok N M, Ha Q P, Nguyen T H, Li J and Samali B 2006 A novel hysteretic model for magnetorheological fluid dampers and parameter identification using particle swarm optimization *Sensors Actuators* A **132** 441–51

Sapiński B 2010 Vibration power generator for a linear MR damper *Smart Mater. Struct.* **19** 1050–62

Scruggs J T and Lindner D 1999 Active energy control in civil structure *Proc. SPIE Conf. on Smart Systems for Bridges, Structures and Highways*; *Proc. SPIE* **3671** 194

Wang W H, Bai X X and Liao W H 2010 An integrated relative displacement self-sensing magnetorheological: prototyping and testing *Smart Mater. Struct.* **19** 105008

Wang Z, Chen Z and Spencer B F Jr 2009 Self-powered and sensing control system based on MR damper: presentation and application *Proc. SPIE Smart Structures/NDE*; *Proc. SPIE* **7292** 729240